Modular Hierarchical Model Predictive Control for Coordinated and Holistic Energy Management of Buildings

Mario Vašak, *Member, IEEE*, Anita Banjac, *Member, IEEE*, Nikola Hure, *Member, IEEE*, Hrvoje Novak, *Member, IEEE*, Danko Marušić, *Student Member, IEEE*, and Vinko Lešić, *Senior Member, IEEE*

***Abstract*—Modular building energy management strategy based on a three-level hierarchical model predictive control is proposed in the paper. Building zones, central medium conditioning and microgrid subsystems are controlled independently by individual linear and nonlinear model predictive controllers, and further integrated together as levels of hierarchical coordination control structure based on price-consumption information exchange. The three-level coordination provides a holistic energy management strategy and enables significant demand response ancillary services for buildings as prosumers, while retaining the independence of required expertise in very different building subsystems. The approach is applied for daily operation scheduling of a full-scale building consisting of 248 offices. Models of building subsystems are obtained by identification procedures on measurement data. Compared to rule-based control, detailed realistic simulations show that the overall building operation cost for typical days in summer is reduced by 9-12% for level-by-level energy-optimal and by 15-24% for price-optimal, coordinated operation. The application of predictive control in the proposed way also improves the indoor comfort substantially.**

***Index Terms*—Building energy management system, central medium conditioning, zone comfort control, energy efficiency, hierarchical coordination, microgrid energy management, model predictive control, price-optimal control.**

I. Introduction

ADVANCED control systems for buildings energy management have emerged as promising tools to significantly increase the energy efficiency, motivated by the fact of 30% of global energy consumption being spent for buildings operation, and by a 20% rise in energy demand of the sector over the last 17 years [1]. With the development of reduced-complexity accurate building thermal models, a great potential is discovered in model predictive control (MPC) as a control method for systematic improvements in energy savings or operational cost reductions in various building subsystems.

Starting with high theoretical energy saving potential, of up to 70% in particular applications [2]–[4], MPC approaches resulted with experimentally validated building energy efficiency increase by 17% in a comprehensive building automation case study [5], 29% of heating, ventilation, and air conditioning (HVAC) electricity and 63% of thermal energy savings in [6], up to 20% electricity savings in [7], or recently with 25% increased energy efficiency and 72% improved comfort by combining decision trees approach for modeling and MPC for optimal decisions [8]. In addition to zone climate control, the MPC approach adds to increased savings of 13% when applied to heat pump [9], with load shifting by up to 61% [10], [11] and to peak electricity power reduction by 35-72% [2].

Recently, a large potential is recognized in merging advanced control with distributed energy resources in energy grids by observing buildings as active entities capable of providing various ancillary services, i.e. as prosumers. Buildings act as thermo-electric storage systems, which are identified as the main need for integration of large share of renewable energy sources [12]. In particular, a mixed-integer linear MPC in microgrid control achieves 35% savings for the considered configuration and experimental operation in [13]. A genetic algorithm for battery storage optimization in [14] reduced grid-supplied energy to the considered building by 13%. In [15], the application of modular hierarchical coordination between predictive zones control and energy flows in the building microgrid ensured 123% savings (revenue equal to 23% of the baseline cost) on a yearly scale.

Despite the promising and thoroughly validated results, a commercial application based on MPC is still not available. Required expert knowledge and staff costs are among the main identified reasons [5]. Buildings are complex systems composed of many coupled subsystems responsible for maintaining safe and efficient operation. These subsystems are often very different in dynamics, mathematical models types, priorities, means of operation but also implementation aspects such as energy levels, protocols, maintenance services, etc. Typical applications of a building energy management system (BEMS) neglect cooperation among all constituent subsystems, resulting in uncoordinated and non-optimal behavior of the building as

Manuscript received April 29, 2020; revised September 23, 2020, April 3, 2021, and September 9, 2021; accepted September 16, 2021. Date of publication September 28, 2021; date of current version November 23, 2021. This work was supported by European Union Regional Development Fund via Operational Programme Competitiveness and Cohesion for Croatia through the Project PC-ATE Buildings – Development of a System for Predictive Control and Autonomous Trading of Energy in Buildings under Contract KK.01.2.1.01.0069. Paper no. TEC-00262-2020. *(Corresponding author: Mario Vašak.)*

The authors are with the University of Zagreb, Faculty of Electrical Engineering and Computing, Laboratory for Renewable Energy Systems, HR-10000 Zagreb, Croatia (e-mail: mario.vasak@fer.hr; anita.banjac@fer.hr; nikola.hure@fer.hr; hrvoje.novak@fer.hr; danko.marusic@fer.hr; vinko.lesic@fer.hr).

Color versions of one or more figures in this article are available at https://doi.org/10.1109/TEC.2021.3116153.

Digital Object Identifier 10.1109/TEC.2021.3116153

a whole. However, as a method, the MPC is suitable both for flexible integration of various technologies that achieve optimal operation of individual subsystems and for the overall coordination.

To this aim, we introduce a hierarchical three-level optimization of building subsystems as independent modules: (A) building zones level, (B) central HVAC system level, and (C) building microgrid level, mutually coordinated by a parametric MPC approach. The subsystems are separated in a hierarchical fashion [15], [16] rather than having a single complex control problem. In the multi-level control topology, comfort criteria, thermal energy and electricity are concurrently optimized while balancing microgrid energy flows, in presence of variable weather, user behavior (occupancy, consumption) and electricity market conditions. At the same time, hierarchical topology enables easier implementation and retains level-specific practice such as equipment, protocols and staff. In particular, (C) introduces a possibility to manage energy storages, energy conversion systems and controllable loads on the building level, (B) introduces a central heating or cooling medium conditioning and (A) delivers the users comfort. Coordinated operation of all levels ensures the price-optimal behavior of the whole building with ensured end-users comfort. Interaction with the grid further enables the building to become an active entity in a smart district or smart grid.

The outputs of the coordination procedure within such a BEMS are further passed as references to corresponding BEMS interfaces acting as links between the BEMS and the building automation system, e.g. room controllers [17] on the zones level, chiller controller [16] on the central HVAC system level or battery system power converter controllers [18] on the microgrid level.

The proposed approach is applied to a full-scale case study building of 248 controllable building zones with two-pipe fan coil units, the HVAC system operating in a cooling season and a microgrid comprising lithium-ion battery storage system with fully controllable power converter and a photovoltaic system. Verification of achievable benefits in daily operation scheduling is performed with a mathematical model of the building and its subsystems identified based on the on-site data, historical weather data measurements and relevant energy pricing conditions [19], [20].

The following contributions of the paper are highlighted:

- modular hierarchical three-level MPC for global coordination through predicted optimal operations and cost sensitivities of hierarchy levels;
- holistic building optimization through coordinated BEMS operation on a real case-study building with its models tuned based on measurements, showing substantial operational costs reduction and indoor comfort increase compared to the performance of industrial state-of-the-art building controls.

The paper is organized as follows. BEMS based on MPC is described in Section II. Section III presents the hierarchical coordination between the optimization levels. In Section IV, the approach is demonstrated on a smart building case study, with substantial savings achieved and reported.

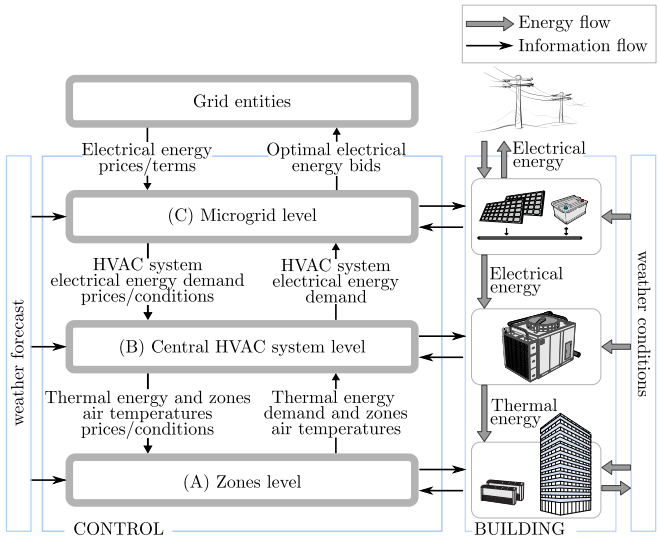

Fig. 1. The proposed modular decomposition and hierarchical coordination in a building.

II. Building Energy Management System

The considered Building Energy Management System (BEMS) consists of three levels following the building energy system vertical decomposition in its major parts: (A) zones level, (B) central HVAC system level, and (C) microgrid level (Fig. 1). The inter-level interactions are later on more formally mathematically treated and explained. In essence, for direction up a level provides predictions of its own behaviour in variables relevant for the first upper level decision-making. In direction down a level provides sensitivity of its own optimal cost and optimizer for set-localized changes of the level-down predicted behaviour.

The most significant property of the proposed concept is modularity where each of the introduced levels may operate independently, in a standalone way. Previously controllable loads in this case now become passive, non-controllable loads and opportunity for cost savings is therefore not fully exploited, but the remaining levels operate to achieve best cost for the building operation in such a constellation.

Predictive control optimization problems for zones, central HVAC system and microgrid control levels are described in the sequel; superscripts 'z,' 'h' and 'μ,' respectively denote variables from these levels. Lower and uppercase letters are used to denote vectors and matrices, respectively, while bold notation is used to denote variables stacked over the prediction horizon of length N. Appropriately sized (column) vectors of ones and zeros are denoted with $\mathbf{1}$ and $\mathbf{0}$, respectively. Notation '*' in the superscript denotes the values obtained by optimization.

A. Zones Level Optimal Control for High Comfort Demands

The recent studies on MPC applied for zone temperature control are divided into two categories. The optimization criteria used in the first category of studies is mainly focused on minimizing the use and cost of energy, while the zone temperature is constrained to be within a considerably large interval. Productivity of occupants in commercial buildings depends largely

on comfort levels, but also on lots of subjective factors [21], [22], so the second category of studies focuses not only on controlling the energy consumption for reducing cost but also on user comfort. The comfort is typically included directly into the optimization criteria through penalization of temperature deviation from user-defined temperature reference [23] or a more complex metric for defining the user comfort is used, like e.g. Predicted Mean Vote index [22], [24]. The zone temperature control approach considered in the paper allows the individual setting of comfort level with the aim of user satisfaction and increased productivity weighed at the same time with energy savings. This is enabled by the applied direct control of thermal energy inputs per zone [17]. For this reason, the methodology is further readily applicable for different heating/cooling elements in zones and open for interaction with the upper levels.

1) Discrete-Time System Model: Zone temperature dynamics is described with a linear state-space model of the following form:

$$\begin{aligned} x^{\mathrm{z}}_{k+1} &= A^{\mathrm{z}} x^{\mathrm{z}}_k + B^{\mathrm{z}}_d d^{\mathrm{z}}_k + B^{\mathrm{z}}_u u^{\mathrm{z}}_k, \\ y^{\mathrm{z}}_k &= C^{\mathrm{z}} x^{\mathrm{z}}_k, \end{aligned} \tag{1}$$

where $k \in \mathbb{Z}$ represents the discrete-time index, $x^{\mathrm{z}}_k \in \mathbb{R}^{n^{\mathrm{z}}_x}$ denotes the zone level state vector consisting of zones air temperature states and additional states modelling the thermal behaviour of higher thermal capacity elements, $y^{\mathrm{z}}_k \in \mathbb{R}^{n^{\mathrm{z}}_y}$ is an output vector consisted of zones air temperatures, $u^{\mathrm{z}}_k \in \mathbb{R}^{n^{\mathrm{z}}_u}$ is a vector of thermal energy inputs into each of $n^{\mathrm{z}}_u = n^{\mathrm{z}}_y$ controllable zones and $d^{\mathrm{z}}_k \in \mathbb{R}^{n^{\mathrm{z}}_d}$ is the disturbance input (outdoor temperature, solar irradiance, internal gains, etc.). Positive values of u^{z}_k represent heating, while negative u^{z}_k stands for cooling. Energies with index k like u^{z}_k generally in the paper represent energies realized in period $[kT_s, (k+1)T_s)$ where T_s is the sampling time for models discretization. Matrices A^{z}, B^{z}_d, B^{z}_u and C^{z} are of appropriate dimensions and are obtained based on a grey-box modeling approach which is detailed in [25].

2) Optimization Problem: Users' comfort is defined by a temperature reference sequence $\mathbf{y}^{\mathrm{z}}_{\mathrm{ref}} \in \mathbb{R}^{N \cdot n^{\mathrm{z}}_y}$ and a permissible zone temperature interval defined with $\pm\boldsymbol{\Delta}^{\mathrm{z}}_{\mathrm{ref}} \in \mathbb{R}^{N \cdot n^{\mathrm{z}}_y}$:

$$\mathbf{y}^{\mathrm{z}}_{\mathrm{ref}} - \boldsymbol{\Delta}^{\mathrm{z}}_{\mathrm{ref}} - \boldsymbol{\sigma} \leq \mathbf{y}^{\mathrm{z}} \leq \mathbf{y}^{\mathrm{z}}_{\mathrm{ref}} + \boldsymbol{\Delta}^{\mathrm{z}}_{\mathrm{ref}} + \boldsymbol{\sigma}, \tag{2}$$

where $\boldsymbol{\sigma} \in \mathbb{R}^{N \cdot n^{\mathrm{z}}_y}$ is a vector of non-negative slack variables for highly penalized deviation outside the permissible zone temperature interval that eliminates feasibility problems. The zone heating/cooling element limitations are formulated as:

$$\mathbf{u}^{\mathrm{z}}_{\min} \leq \mathbf{u}^{\mathrm{z}} \leq \mathbf{u}^{\mathrm{z}}_{\max}, \tag{3}$$

where $\mathbf{u}^{\mathrm{z}}_{\min} \in \mathbb{R}^{N \cdot n^{\mathrm{z}}_u}$ and $\mathbf{u}^{\mathrm{z}}_{\max} \in \mathbb{R}^{N \cdot n^{\mathrm{z}}_u}$ are minimum and maximum attainable thermal powers along the prediction horizon, dependent on the current and planned central HVAC system level operation and temperatures within zones [26]. The final optimization problem for energy-saving and comfortable zone temperature control, written in a compact form, is as follows:

$$\begin{aligned} \min_{\mathbf{u}^{\mathrm{z}}, \boldsymbol{\sigma}} \quad & \mathbf{c}^{\top}_{\mathrm{t}} |\mathbf{u}^{\mathrm{z}}| + \gamma \bar{c}_{\mathrm{t}} \boldsymbol{\delta}^{\top} |Q(\mathbf{y}^{\mathrm{z}}_{\mathrm{ref}} - \mathbf{y}^{\mathrm{z}})| + g \mathbf{1}^{\top} \boldsymbol{\sigma}, \\ \text{s.t.} \quad & (1), (2), (3), \boldsymbol{\sigma} \geq \mathbf{0}, \end{aligned} \tag{4}$$

where the operator $|.|$ denotes element-wise absolute value, $\mathbf{c}_{\mathrm{t}} \in \mathbb{R}^{N \cdot n^{\mathrm{z}}_u}$ is the thermal energy cost important for a subsequent coordination with higher level modules, $\bar{c}_{\mathrm{t}} \in \mathbb{R}$ is the mean thermal energy cost, $g \in \mathbb{R}$ is a non-negative weighting parameter for hard penalization of the zone air temperature deviation outside the comfort bounds $\mathbf{y}^{\mathrm{z}}_{\mathrm{ref}} \pm \boldsymbol{\Delta}^{\mathrm{z}}_{\mathrm{ref}}$. The vector $\boldsymbol{\delta} \in \mathbb{R}^{N \cdot n^{\mathrm{z}}_y}$ is the zone occupancy vector, consisted of zeros (indicating vacant zone) and ones (indicating occupied zone). Transformation matrix $Q \in \mathbb{R}^{N \cdot n^{\mathrm{z}}_u \times N \cdot n^{\mathrm{z}}_y}$ stems directly from the dynamic system model as described in [23] and is used to transform the temperature deviation from the reference to the equivalent amount of the required thermal energy input. Energy difference obtained in this way is then multiplied with the mean thermal energy cost $\bar{c}_{\mathrm{t}}$ in order to have both first and second summand in the cost expressed in the same units. The parameter $\gamma \in \mathbb{R}$ is introduced as a tangible weighting parameter for selection of the desired system performance: energy-cost-optimal for $\gamma = 0$, energy cost priority for $0 < \gamma < 1$, equivalent trade-off for $\gamma = 1$ or reference tracking performance priority for $\gamma > 1$.

B. Central HVAC System Level Optimal Control

The considered central HVAC control system is used to condition the thermal medium in the central medium preparation system of the building in a way that minimizes the overall expense for the HVAC system operation while assuring that zones required energies $\mathbf{u}^{\mathrm{z}}$ are attainable and the HVAC electrical load constraints are respected. The central HVAC MPC optimizes setpoints for the central HVAC supply medium temperature [16] along the considered prediction horizon.

The central HVAC level controller is designed in the supervisory control fashion [16]. Specifically, it generates the reference setpoints for the low-level controllers of the central HVAC medium conditioning system that are propagated to the existing building automation system. This approach ensures high safety standards for the system at hand since all the limitations imposed in the low-level industrially developed HVAC controllers remain preserved.

1) Discrete-Time System Model: The considered HVAC system level is derived as a grey-box model and composed of the following subsystems: a chiller, a pipework, a hydraulic pump and fan coil units used to provide thermal energy to zones air. The applied sampling time of 15 minutes allows us to represent the dynamics of the central HVAC system level with a one-step time delay. A brief system description and derived mathematical formulation is given in the sequel, whereas a more detailed model description can be found in [16].

The thermal balance equation for the system at hand at the time-instant k is given by:

$$E^{\mathrm{t,ch}}_k = E^{\mathrm{t,\ losses}}_k + \mathbf{1}^{\top} u^{\mathrm{z}}_k + E^{\mathrm{t,nc}}_k, \tag{5}$$

where $E_k^{\mathrm{t,ch}}$ is the thermal energy consumption of the chiller, $E_k^{\mathrm{t,\ losses}}$ are the thermal losses in the pipework and $E_k^{\mathrm{t,nc}}$ is the non-controllable part of the building thermal loads.

The chiller energy conversion is modelled by energy efficiency ratio (EER), i.e. the ratio of the realized cooling energy with respect to the consumed electrical energy. It is expressed with a nonlinear static function mapping with respect to the ambient air temperature T_o and the thermal load $E^{\mathrm{t,ch}}$, $EER(T_o, E^{\mathrm{t,ch}})$. The EER function parameters are tuned based on a collected set of historical measurements of chiller operation in the case-study building.

Distribution of the pipeline flows and fan coil units within the building is considered in the model to enable estimation of attainable energies in the zones and incurred thermal losses in the cooling medium distribution. The model also incorporates the nonlinear attainable thermal energy functions of the fan coil units with respect to supply medium temperature and room air temperature and the associated electrical energy consumption functions for fan coils fans.

All of the above is described by a nonlinear input-output model:

$$y_k^{\mathrm{h}} = h^{\mathrm{h}}(u_{k-1}^{\mathrm{h}}, [u_k^{\mathrm{z}\top}, y_k^{\mathrm{z}\top}]^\top, d_k^{\mathrm{h}}), \tag{6}$$

where $y_k^{\mathrm{h}} \in \mathbb{R}$ is the HVAC level electrical energy consumption, $u_k^{\mathrm{h}} \in \mathbb{R}$ is the starting cooling medium temperature and $d_k^{\mathrm{h}} = [T_{\mathrm{o},k}\ E_k^{\mathrm{t,nc}}]^\top$. A one-step delay is incorporated in the model to take into account the inherited delays of the decision variable propagation through the chiller control loops and the induced delays due to the thermal capacity of the pipework.

1) Optimization Problem: The controller is formulated in the form of MPC, with the associated optimization problem given by [16]:

$$\min_{\mathbf{u}^{\mathrm{h}}} \quad \mathbf{c}_{\mathrm{e}}^\top \mathbf{y}^{\mathrm{h}}, \tag{7a}$$

$$\text{s.t.} \quad \mathbf{g}^{\mathrm{h}}(\mathbf{u}^{\mathrm{h}}, [\mathbf{u}^{\mathrm{z}\top}, \mathbf{y}^{\mathrm{z}\top}]^\top, \mathbf{d}^{\mathrm{h}}) \leq \mathbf{0}, \tag{7b}$$

where $\mathbf{c}_{\mathrm{e}} \in \mathbb{R}^N$ is the electrical energy price vector on the prediction horizon and $\mathbf{y}^{\mathrm{h}} \in \mathbb{R}^N$ is the electrical energy consumption profile of the entire HVAC system, including chiller, circulation pumps and fan coils fans electricity consumption. Compact formulation of the optimal control problem constraints is given by the nonlinear vector function $\mathbf{g}^{\mathrm{h}}$. Constraints are imposed on the electrical power consumption of the HVAC level and on the supply medium temperatures required on all fan coils to make their required 15-minutes energies attainable.

The outlined central HVAC system control problem is non-convex and thus solved with a sequential linear programming (SLP) procedure.

D. Microgrid Level Optimal Control

On the microgrid level, the proposed MPC algorithm is utilized on controllable production, storage and consumption units to favorably shape the external energy exchange. In this paper, the battery storage system is considered as the only controllable microgrid element.

1) Discrete-Time System Model: For the MPC implementation, microgrid, i.e. battery storage system dynamics is formulated as:

$$x_{k+1}^{\mu} = A^{\mu} x_k^{\mu} + B^{\mu} u_k^{\mu}, \tag{8}$$

where $x_k^{\mu} \in \mathbb{R}$ is the battery system state-of-energy (SoE), $u_k^{\mu} := [u_{\mathrm{dch},k}^{\mu}\ u_{\mathrm{ch},k}^{\mu}]^\top$ are the battery discharging and charging energies and A^{μ} and B^{μ} are model matrices derived from a linear battery model incorporating constant battery and power converter charge and discharge efficiencies, and a constant battery capacity [27]. The efficiency for battery system charging and discharging is determined experimentally and each of them can be considered flat for the span of energy exchanges that can be performed with the power converter. The actual low efficiency for small power amounts comparable to power converter self-consumption is evaded by using time modulation with higher powers to attain the required energy exchange with the battery within the sampling interval of 15 minutes. The microgrid energy flows are connected via the energy conservation law:

$$y_k^{\mu} = \mathbf{1}^\top u_k^{\mu} + y_k^{\mathrm{h}} + d_{\mathrm{nc},k}^{\mu}, \tag{9}$$

where y_k^{μ} is the electrical energy exchanged with the grid, y_k^{h} is the electrical consumption of the HVAC level described in (6) and $d_{\mathrm{nc},k}^{\mu}$ is the cumulative energy consumption of the system composed of the non-controllable building loads and production units.

2) Optimization Problem: In order to ensure price-optimal operation of the building, the microgrid level optimization problem incorporates the following costs: (i) cost of energy exchanged with the distribution grid, (ii) cost of peak power consumed from the grid and (iii) cost of battery degradation. All of the corresponding costs are summed and the resulting microgrid level cost function is:

$$J^{\mu} = \mathbf{c}_{\mathrm{da}}^\top \mathbf{y}^{\mu} + c_{y_{\max}^{\mu}} \max([y_{\max}^{\mu} \quad 0]) + \mathbf{c}_{\mathrm{bd}}^\top \mathbf{u}^{\mu}, \tag{10}$$

where $\mathbf{c}_{\mathrm{da}}$ is a vector of energy prices along the prediction horizon, $c_{y_{\max}^{\mu}}$ is the fixed cost of maximum power consumption, $y_{\max}^{\mu} = \max(\mathbf{y}^{\mu}/T_{\mathrm{s}})$, where T_{s} is the sampling period, $\max(\cdot)$ denotes the maximum component of a vector and $\mathbf{c}_{\mathrm{bd}}$ is a vector constituted of N times row-wise repeated $[c_{\mathrm{bd,dch}}\ c_{\mathrm{bd,ch}}]$ that contains battery discharging and charging costs obtained from battery degradation properties and its market price [28].

Additional physical constraints are included in order to respect the operational limits specified by the battery and power converter manufacturers such that a safe battery system operation is ensured. Charging and discharging energies within one sampling period are constrained as:

$$\begin{aligned} [u_{\min}^{\mu} \quad 0]^\top \leq u_k^{\mu} \leq [0 \quad u_{\max}^{\mu}]^\top, \\ 0 \leq [1/u_{\min}^{\mu} \quad 1/u_{\max}^{\mu}] u_k^{\mu} \leq 1. \end{aligned} \tag{11}$$

Limits on the energy exchanged with the distribution grid are added as:

$$y_{\min}^{\mu} \leq y_k^{\mu} \leq y_{\max}^{\mu}, \tag{12}$$

and SoE is constrained between the posed operational limits:

$$x_{\min}^{\mu} \leq x_k^{\mu} \leq x_{\max}^{\mu}. \tag{13}$$

The microgrid level optimization problem is then mathematically represented in a compact form as:

$$\min_{\mathbf{u}^{\mu}} \quad J^{\mu}, \qquad \text{s.t.} \quad (8),(9),(11),(12),(13). \tag{14}$$

III. Hierarchical Coordination Between Optimization Levels

The aim of the modular parametric hierarchical coordination is to separate building subsystems in a hierarchical fashion rather than having one large control problem that handles all the subsystems at once. The imposed modularity is based on so called "price-consumption" talk, where the coordination between building subsystems (levels) is attained by communicating the optimized inputs and outputs from the lower hierarchical level (LHL) to the higher hierarchical level (HHL) and the HHL's cost sensitivity and control law in the vicinity of that input/output profile back to the LHL. The cost sensitivity and control law are assessed by utilizing the results from multi-parametric MPC and the notion of critical region (CR) [29]. Hierarchical coordination is performed through revisiting both adjacent levels with the goal of improving the initial LHL solution with respect to the HHL cost, thus transforming it into a global solution for both levels.

The general concept of hierarchical coordination together with its implementation in the BEMS is described in the sequel. Superscripts 'L' and 'H' denote variables related to LHL and HHL, respectively.

A. Parametric Coordination

The initial multi-parametric algorithm [29] is based on a direct exploration of the parameter space starting from a single CR formed around the initial parameter value θ^{H}.

In the case here, parameter θ^{H} is obtained from the set of variables at the optimal solution of the LHL problem.

$$\theta^{\mathrm{H}} = h^{\theta}(\mathbf{u}^{\mathrm{L}*}, \mathbf{y}^{\mathrm{L}*}), \tag{15}$$

where $h^{\theta}(\cdot)$ is a vector function. Important distinction from the multi-parametric MPC approach and the actual algorithm employed here is that only a single CR is determined for the current value of θ^{H}. After the LHL solution $\mathbf{u}^{\mathrm{L}*}$ and $\mathbf{y}^{\mathrm{L}*}$ is obtained, it is used to form parameters θ^{H} of the HHL optimization problem:

$$J^{\mathrm{H}*}(\theta^{\mathrm{H}}) := \min_{\mathbf{u}^{\mathrm{H}}} f^{\mathrm{H}}(\mathbf{x}^{\mathrm{H}}, \mathbf{u}^{\mathrm{H}}, \mathbf{d}^{\mathrm{H}}, \theta^{\mathrm{H}}), \quad \text{s.t.} \begin{cases} (\mathbf{u}^{\mathrm{H}}, \mathbf{x}^{\mathrm{H}}) \in \mathcal{UX}^{\mathrm{H}}(x_0^{\mathrm{H}}, \mathbf{d}^{\mathrm{H}}, \theta^{\mathrm{H}}), \\ \theta^{\mathrm{H}} = h^{\theta}(\mathbf{u}^{\mathrm{L}*}, \mathbf{y}^{\mathrm{L}*}), \\ \mathbf{x}^{\mathrm{H}} = h^{\mathrm{H}}(x_0^{\mathrm{H}}, \mathbf{u}^{\mathrm{H}}, \mathbf{d}^{\mathrm{H}}), \end{cases} \tag{16}$$

where $f^{\mathrm{H}}(\cdot)$ is a convex piecewise affine cost function, $\mathbf{u}^{\mathrm{H}}$, $\mathbf{x}^{\mathrm{H}}$, $\mathbf{d}^{\mathrm{H}}$ and $\mathcal{UX}^{\mathrm{H}}$ are HHL inputs, states and disturbances as well as the corresponding input-state feasible set, $h^{\theta}(\cdot)$ is a vector function and $h^{\mathrm{H}}(\cdot)$ represents the HHL system dynamics. By applying the geometric multi-parametric algorithm from [29], a single polytopic CR is computed around θ^{H} directly from the solution of the mathematical program (16) as will be shown in the sequel. In it, the control law $\mathbf{u}^{\mathrm{H}*}(\theta^{\mathrm{H}})$ and the value function $J^{\mathrm{H}*}(\theta^{\mathrm{H}})$ are affine with respect to θ^{H}. A CR is a subset of parameters θ^{H} that yield the same set of active constraints, i.e. constraints that are satisfied with equality, in the optimal solution of (16). Therefore, constraints on $\mathbf{u}^{\mathrm{H}}$ from (16) are written in a matrix form and parted into an active (A) and an inactive (NA) subset for a certain CR, with optimal control law $\mathbf{u}^{\mathrm{H}*}$:

$$G_{\mathrm{A}}^{\mathrm{H}}\mathbf{u}^{\mathrm{H}*}(\theta^{\mathrm{H}}) = w_{\mathrm{A}}^{\mathrm{H}} + E_{\mathrm{A}}^{\mathrm{H}}\theta^{\mathrm{H}}, \tag{17}$$

$$G_{\mathrm{NA}}^{\mathrm{H}}\mathbf{u}^{\mathrm{H}*}(\theta^{\mathrm{H}}) < w_{\mathrm{NA}}^{\mathrm{H}} + E_{\mathrm{NA}}^{\mathrm{H}}\theta^{\mathrm{H}}, \tag{18}$$

where G^{H}, w^{H} and E^{H} are matrices obtained from the constraints in (16). The affine optimal control law for the optimizer and the corresponding affine cost function with respect to the parameter θ^{H}, called value function, follow from (17) and are formulated as:

$$\mathbf{u}^{\mathrm{H}*}(\theta^{\mathrm{H}}) = \underbrace{(G_{\mathrm{A}}^{\mathrm{H}})^{-1}E_{\mathrm{A}}^{\mathrm{H}}}F^{\mathrm{H,CR}}\theta^{\mathrm{H}} + \underbrace{(G_{\mathrm{A}}^{\mathrm{H}})^{-1}w_{\mathrm{A}}^{\mathrm{H}}}q^{\mathrm{H,CR}},$$

$$\theta^{\mathrm{H}} \in \mathrm{CR}, \tag{19}$$

$$J^{\mathrm{H}*}(\theta^{\mathrm{H}}) = h^{\mathrm{H,CR}}\theta^{\mathrm{H}} + f^{\mathrm{H,CR}}, \quad \theta^{\mathrm{H}} \in \mathrm{CR}, \tag{20}$$

$$\mathrm{CR} = \{\theta^{\mathrm{H}} | G^{\mathrm{H,CR}}\theta^{\mathrm{H}} \leq w^{\mathrm{H,CR}}\}, \tag{21}$$

where coefficients $h^{\mathrm{H,CR}}$ and $f^{\mathrm{H,CR}}$ are obtained by substituting the control law from (19) into the cost function from (16). The CR boundaries $G^{\mathrm{H,CR}}$ and $w^{\mathrm{H,CR}}$ are calculated as:

$$G^{\mathrm{H,CR}} = G_{\mathrm{NA}}^{\mathrm{H}}F^{\mathrm{H,CR}} - E_{\mathrm{NA}}^{\mathrm{H}},$$

$$w^{\mathrm{H,CR}} = w_{\mathrm{NA}}^{\mathrm{H}} - G_{\mathrm{NA}}^{\mathrm{H}}q^{\mathrm{H,CR}}.$$

In case of the CR degeneracy, additional steps are required to obtain a full-dimensional non-degenerate CR. When a primal degenerate CR is obtained, depending on the primal degeneracy case, either the active constraints subset is reduced using e.g. QR decomposition, or the initial θ^{H} is randomly permuted such that a full-dimensional CR, including the initial θ^{H}, is obtained [29]. For the case of dual degeneracy, a particular optimizer is chosen on a vertex of the feasible solutions set of the HHL [29] as an inherent solver characteristic.

The calculated CR, value function and control law are then passed to the LHL in order to reoptimize the previously obtained LHL solution:

$$J^{\mathrm{L}*} := \min_{\mathbf{u}^{\mathrm{L}}} J^{\mathrm{H}*}(\theta^{\mathrm{H}}) + f^{\mathrm{L}}(\mathbf{x}^{\mathrm{L}}, \mathbf{u}^{\mathrm{L}}, \mathbf{d}^{\mathrm{L}}), \quad \text{s.t.} \begin{cases} (\mathbf{u}^{\mathrm{L}}, \mathbf{x}^{\mathrm{L}}) \in \mathcal{UX}^{\mathrm{L}}(x_0^{\mathrm{L}}, \mathbf{d}^{\mathrm{L}}, \mathbf{u}^{\mathrm{H}*}(\theta^{\mathrm{H}})), \\ \mathbf{x}^{\mathrm{L}} = h^{\mathrm{L}}(x_0^{\mathrm{L}}, \mathbf{u}^{\mathrm{L}}, \mathbf{d}^{\mathrm{L}}), \\ \theta^{\mathrm{H}} = h^{\theta}(\mathbf{u}^{\mathrm{L}}, \mathbf{y}^{\mathrm{L}}) \in \mathrm{CR}, \end{cases} \tag{22}$$

where $f^{\mathrm{L}}(\cdot)$ is a convex piecewise affine cost function of the LHL which includes the cost terms that are not coordinated between levels (e.g. comfort terms in (4)), $\mathbf{u}^{\mathrm{L}}$, $\mathbf{x}^{\mathrm{L}}$, $\mathbf{d}^{\mathrm{L}}$ and $\mathcal{UX}^{\mathrm{L}}$ are the LHL inputs, states and disturbances as well as the corresponding input-state feasible set, and $h^{\mathrm{L}}(\cdot)$ represents the LHL system dynamics.

The hierarchical coordination is continued with respect to the constraints activated at the optimal solution of the LHL problem (22) where the following cases can appear (see Fig. 2):

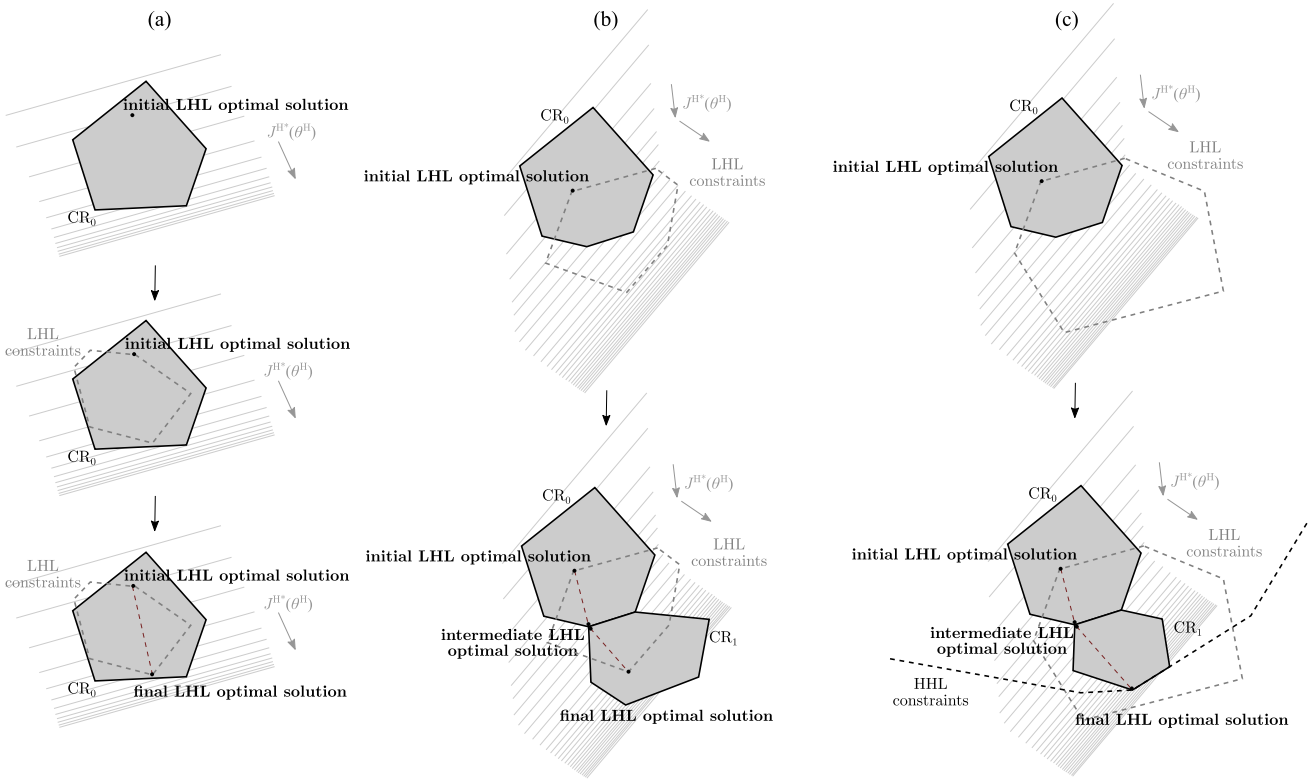

Fig. 2. Possible algorithm outcomes with respect to the CR constraints activation where: (a) only a single CR is calculated, (b) where CR boundaries are reached and a new CR exists over the boundary and (c) where CR boundaries are reached and no CR exists over the boundary.

1: At least one CR constraint is activated: (16) is solved again with the new values of $\mathbf{u}^{\mathrm{L}*}$ and $\mathbf{y}^{\mathrm{L}*}$ in the adjacent CR,
   1.1: if the adjacent CR exists, its description and new affine value function and control law for it are computed and passed to (22) Fig. 2(b) and (c),
   1.2: if no adjacent CR exists, the optimum is reached and the procedure concludes Fig. 2(c) - bottom part),
2: No CR constraint is activated: the optimum is reached and the procedure concludes Fig. 2(a) and (b) - bottom part).

B. Coordination Between BEMS Optimization Levels

During coordination within the BEMS, building optimization levels exchange information through respective value function, control law and boundary constraints of the CR. The zone level communicates to the central HVAC system level the optimized profiles of thermal energy consumption and air temperatures within zones. The central HVAC system level optimizes its behavior with respect to the obtained zones profiles and communicates back the CR, value function and control law for starting medium temperature, with respect to zones thermal energies and air temperatures. Coordination between the microgrid and the HVAC levels is achieved by communicating the overall HVAC system electrical energy consumption profile to the microgrid level and local characterization of the electrical energy cost function from the microgrid to the HVAC level. BEMS operation scheme is in Fig. 1 and in (23)–(25).

1) Microgrid Level Problem:

$$J^{\mu*}(\theta^{\mu}) := \min_{\mathbf{u}^{\mu}} J^{\mu}(\theta^{\mu}, \mathbf{u}^{\mu}, \mathbf{x}^{\mu}, \mathbf{d}^{\mu}),$$
$$\text{s.t.} \begin{cases} (\mathbf{u}^{\mu}, \mathbf{x}^{\mu}) \in \mathcal{UX}^{\mu}(x_0^{\mu}, \mathbf{d}^{\mu}, \theta^{\mu}), \\ \theta^{\mu} = \mathbf{y}^{\mathrm{h}*}, \\ \mathbf{x}^{\mu} = h^{\mu}(x_0^{\mu}, \mathbf{u}^{\mu}, \mathbf{d}^{\mu}), \end{cases} \tag{23}$$

where $J^{\mu}(\cdot)$ is the cost function from (14) presented here in a generalized form for convenience, $\mathbf{y}^{\mathrm{h}*}$ is the optimized output vector of the central HVAC system level, utilized as a parameter vector on the microgrid level, $\mathbf{u}^{\mu}$ and $\mathbf{x}^{\mu}$ are the microgrid input and state vectors with x_0^{μ} denoting the initial system state, the corresponding feasible set $\mathcal{UX}^{\mu}$ consists of microgrid physical constraints and systems dynamics $h^{\mu}(\cdot)$ given in (8), (9), (11), (12), (13).

2) Problem of the Central HVAC System Level:

$$J^{\mathrm{h}*}(\theta^{\mathrm{h}}) := \min_{\mathbf{u}^{\mathrm{h}}} J^{\mu*}(\theta^{\mu}),$$
$$\text{s.t.} \begin{cases} \theta^{\mu} = \mathbf{y}^{\mathrm{h}}, \\ \mathbf{u}^{\mathrm{h}} \in \mathcal{U}^{\mathrm{h}}(\theta^{\mathrm{h}}, \mathbf{d}^{\mathrm{h}}), \\ \theta^{\mathrm{h}} = [\mathbf{u}^{\mathrm{z}*\top}\ \mathbf{y}^{\mathrm{z}*\top}]^{\top}, \\ \mathbf{y}^{\mathrm{h}} = h^{\mathrm{h}}(\mathbf{u}^{\mathrm{h}}, \theta^{\mathrm{h}}, \mathbf{d}^{\mathrm{h}}), \\ \mathbf{y}^{\mathrm{h}} \in \mathcal{C}^{\mu}, \end{cases} \tag{24}$$

where the set $\mathcal{U}^{\mathrm{h}}(\theta^{\mathrm{h}})$ arises from the central HVAC system level constraints along the prediction horizon (7b) and $\mathcal{C}^{\mu}$ is the microgrid level CR. Electrical energy consumption of the HVAC level $\mathbf{y}^{\mathrm{h}}$ is the parameter θ^{μ} on the microgrid level, whereas

Algorithm 1: Modular hierarchical parametric MPC for coordinated BEMS operation.

initialization:

$$J^{\mathrm{h}*(-1)} = \|\cdot\|_1, J^{\mu*(-1)} = \|\cdot\|_1, \mathbf{u}^{\mathbf{h}*-\mathbf{1}},$$

$$\mathcal{C}^{\mathrm{h}(-1)} = \mathbb{R}^{N\cdot(n_{\mathrm{u}}^{\mathrm{z}}+n_{\mathrm{y}}^{\mathrm{z}})}, \mathcal{C}^{\mu(-1)} = \mathbb{R}^{N},$$

i=0

repeat:

1: zones (25): $J^{\mathrm{h}*(i-1)}$, $\mathbf{u}^{\mathrm{h}*(i-1)}$ and $\theta^{\mathrm{h}} \in \mathcal{C}^{\mathrm{h}(i-1)} \rightarrow \theta^{\mathrm{h}*(i)}$;

2: central HVAC system (24): $J^{\mu*(i-1)}, \theta^{\mathrm{h}} = \theta^{\mathrm{h}*(i)}$ and $\theta^{\mu} \in \mathcal{C}^{\mu(i-1)} \rightarrow \theta^{\mu*(i)}$;

3: microgrid (23): $\theta^{\mu} = \theta^{\mu*(i)} \rightarrow \mathcal{C}^{\mu(i)}$, $J^{\mu*(i)}$;

4: central HVAC system (24): $J^{\mu*(i)}, \theta^{\mathrm{h}} = \theta^{\mathrm{h}*(i)}$ and $\theta^{\mu} \in \mathcal{C}^{\mu(i)} \rightarrow \mathcal{C}^{\mathrm{h}(i)}$, $J^{\mathrm{h}*(i)}$, $\mathbf{u}^{\mathrm{h}*(i)}(\theta^{\mathrm{h}})$;

5: $i = i + 1$;

until no CRs constraints are activated or no new CR over the boundary.

parameter θ^{h} on the central HVAC system level are the thermal energy and air temperature profiles obtained on the zone level.

3) Zone level problem is:

$$J^{\mathrm{z}*} := \min_{\mathbf{u}^{\mathrm{z}},\boldsymbol{\sigma}} J^{\mathrm{h}*}(\theta^{\mathrm{h}}) + f^{\mathrm{z}}(\overline{c}_{\mathrm{t}}, \mathbf{u}^{\mathrm{z}}, \mathbf{x}^{\mathrm{z}}, \boldsymbol{\sigma}, \mathbf{d}^{\mathrm{z}}),$$

$$\text{s.t.} \begin{cases} (\mathbf{u}^{\mathrm{z}}, \mathbf{x}^{\mathrm{z}}) \in \mathcal{UX}^{\mathrm{z}}(x_0^{\mathrm{z}}, \mathbf{u}^{\mathrm{h}*}(\theta^{\mathrm{h}}), \mathbf{d}^{\mathrm{z}}), \\ \mathbf{x}^{\mathrm{z}} = h^{\mathrm{z}}(x_0^{\mathrm{z}}, \mathbf{u}^{\mathrm{z}}, \mathbf{d}^{\mathrm{z}}), \\ \theta^{\mathrm{h}} = [\mathbf{u}^{\mathrm{z}\top}\ \mathbf{y}^{\mathrm{z}\top}]^{\top}, \\ \theta^{\mathrm{h}} \in \mathcal{C}^{\mathrm{h}}, \\ \mathbf{y}_{\mathrm{ref}}^{\mathrm{z}} - \boldsymbol{\Delta}_{\mathrm{ref}}^{\mathrm{z}} - \boldsymbol{\sigma} \le \mathbf{y}^{\mathrm{z}} \le \mathbf{y}_{\mathrm{ref}}^{\mathrm{z}} + \boldsymbol{\Delta}_{\mathrm{ref}}^{\mathrm{z}} + \boldsymbol{\sigma}, \\ \boldsymbol{\sigma} \ge \mathbf{0}, \end{cases} \tag{25}$$

where $f^{\mathrm{z}}(\cdot)$ is the comfort-related part of the zone level cost function described in (4) presented here in a generalized form for convenience, $\overline{c}_{\mathrm{t}}$ is the mean price of the thermal energy in all building zones, $\mathbf{u}^{\mathrm{z}}$ and $\mathbf{x}^{\mathrm{z}}$ are the input and state vectors with x_0^{z} denoting the initial system state, the corresponding feasible set $\mathcal{UX}^{\mathrm{z}}$ consists of zone physical constraints and system dynamics $h^{\mathrm{z}}(\cdot)$ and is described with (1) and (3). After the initial coordination iteration, CR of the central HVAC system level encompasses the thermal energy limit constraints, so the zone thermal constraints (3) used in the initial iteration with presumed minimal supply temperatures from the central HVAC system level can be omitted from the set $\mathcal{UX}^{\mathrm{z}}$ in the subsequent iterations. The set $\mathcal{C}^{\mathrm{h}}$ represents the CR of the central HVAC system level.

Coordination algorithm can then be described using the general formulation of different levels optimizations from (23)–(25), as presented in Algorithm 1. In Algorithm 1 iterations are denoted with i, and index i in brackets in the variable superscript denotes the corresponding variable value in the ith iteration.

Coordination algorithm is initialized by performing the first pass through all the considered levels based on an energy-optimal criterion for zone and central HVAC system level and corresponding CRs initialized as $\mathcal{C}^{\mathrm{h}} = \mathbb{R}^{N\cdot(n_{\mathrm{u}}^{\mathrm{z}}+n_{\mathrm{y}}^{\mathrm{z}})}$ and $\mathcal{C}^{\mu} = \mathbb{R}^{N}$, denoting an unbounded set of real numbers with the corresponding dimensions. At the initial iteration of the algorithm the optimization vector of the central HVAC system level $\mathbf{u}^{\mathrm{h}*(-1)}$ is for the case of cooling initialized with the lowest admissible values of the supply medium temperature reference.

The results of the zone level optimization are zone temperatures $\mathbf{y}^{\mathrm{z}*}$ and the required optimal thermal energies $\mathbf{u}^{\mathrm{z}*}$ that need to be supplied to the zones, stacked into the parameter $\theta^{\mathrm{h}*(i)}$ and passed to the central HVAC system level.

The central HVAC system level controller uses the current value of the parameter vector $\theta^{\mathrm{h}*(i)}$ and finds the optimal solution to the problem (24). The optimized control profile at the central HVAC system level results with the electrical energy consumption profile $\theta^{\mu*(i)} = \mathbf{y}^{\mathrm{h}*}$ which is propagated to the microgrid level. In the first execution of the central HVAC system level is (24) solved as energy-optimal control problem, since the electricity prices from the microgrid level are not available at the given time. In the following executions are the electricity prices determined by the currently active CR at the microgrid level, i.e. with the associated cost function $J^{\mu*(i-1)}$ and constraints $\mathcal{C}^{\mu(i-1)}$.

In the next step microgrid level computes the optimal control policy around the declared HVAC consumption profile $\theta^{\mu*(i)}$ and provides the central HVAC system with the cost description $J^{\mu*(i)}$ and boundaries $\mathcal{C}^{\mu(i)}$ of the respective CR.

Following the microgrid level optimization execution, the central HVAC system level optimizes its operation based on the latest declared zone requests and the obtained prices and boundaries from the microgrid level. It also computes the value function $J^{h*(i)}$ and CR $\mathcal{C}^{h(i)}$ associated with the optimized control profile and makes them available to the zones level in the next iteration of the algorithm.

The coordination is performed iteratively until no CR constraints are activated (as presented in Fig. 2(a) and (b)) or there is no new CR existent over the boundary (as presented in Fig. 2(c)) simultaneously in both interactions between levels, in which cases the algorithm is concluded. In cases where the CR boundaries are reached, the parameter $\theta^{(i)}$ is transferred over the activated CR boundary in the direction that decreases the corresponding CR value function $J^{*(i)}(\theta)$ through:

$$\theta^{(i+1)} = \theta^{(i)} - \epsilon h^{\mathrm{CR}(i)}, \tag{26}$$

where $h^{\mathrm{CR}(i)}$ is the gradient of the CR value function $J^{*(i)}(\theta)$ as in (20) and ϵ is a parameter of small value (e.g. solver precision or 1% of $\|h^{\mathrm{CR}(i)}\|_1$) chosen to ensure entering into the adjacent CR (if it exists).

IV. Validation of the Developed Building Energy Management System

The 13-floors skyscraper building of University of Zagreb Faculty of Electrical Engineering and Computing, which is also a protected cultural heritage [30], is here used as a case study. The building consists of 248 controllable zones equipped with two-pipe fan coil units (FCUs) for seasonal heating or cooling and is equipped with BEMS [31]. The building has roughly 10.000 m^2 of useful area and zones windows are oriented either

TABLE I
THE CASE STUDY AND THE CONSIDERED SIMULATION SCENARIO

Description	Notation	Value
Zone temp. setpoint, allowed deviation	$y^{\mathrm{z}}_{\mathrm{ref}}$, $\Delta^{\mathrm{z}}_{\mathrm{ref}}$	24°C, 1.5°C
Chiller rated power (electrical)	–	244.2 kW
Max. chiller supply temperature	$u^{\mathrm{h}}_{\max}$	15.6°C
Min. chiller supply temperature	$u^{\mathrm{h}}_{\min}$	7°C
Battery capacity	–	32 kWh
Battery discharge efficiency	–	93%
Battery charge efficiency	–	96%
Min./Max battery energy state	$x^{\mu}_{\min}$, $x^{\mu}_{\max}$	10%, 90%
Max. battery energy discharge in 15 min.	$u^{\mu}_{\min}$	-2.4 kWh
Max. battery energy charge in 15 min.	$u^{\mu}_{\max}$	2.4 kWh
Max. grid energy in 15 min. (selling)	$y^{\mu}_{\min}$	-90 kWh
Max. grid energy in 15 min. (buying)	$y^{\mu}_{\max}$	90 kWh
Photovoltaic plant power rating	–	10.58 kWp
Battery degradation cost	$\lvert c_{\mathrm{bd}}\rvert$	0.226 €/kWh
Maximum power cost	$c_{y^{\mu}_{\max}}$	0.116 €/kW

to the south or to the north. The identified semi-physical model of the case-study building consists of identified second-order models [25] of all 248 controllable zones ($n^{\mathrm{z}}_u = n^{\mathrm{z}}_y = 248$, $n^{\mathrm{z}}_x = 2n^{\mathrm{z}}_y$) stacked into the compact model form (1). Disturbance vector $d^{\mathrm{z}}_k \in \mathbb{R}^{n^{\mathrm{z}}_d}$ ($n^{\mathrm{z}}_d = n^{\mathrm{z}}_u + 9$) is a vector of predicted equivalent heat disturbance for each zone[1] and of external weather influences affecting the building temperature behavior, consisted of outside air temperature and diffuse and direct solar irradiances incident on the exterior building surfaces.

The GWL Power Group Lithium Cell batteries [32] energy storage system is located in the building basement with overall storage capacity of 32 kWh and 89% round-cycle efficiency. It is connected to the building grid with a fully controllable power converter with a power rating of 9.6 kW. Building rooftop photovoltaic (PV) plant is comprised of 3 PV arrays, each with 15 poly-Si PV panels (Solvis SV60-235) connected in series, amounting to overall PV plant power of 10.58 kW in standard test conditions (10.58 kWp). The building energy exchange with the grid is limited by the power rating of 2 building transformers (20/0.4 kV). Relevant meteorological conditions are measured by the meteorological station on the building rooftop and specifically the direct and diffuse solar irradiance components are measured by Kipp and Zonen CHP1 pyrheliometer and CMP11 pyranometer, respectively, both mounted on a Solys2 sun tracker with a sun sensor for active tracking.

The building temperature is controlled within comfort interval of 24 ± 1.5 °C during occupied periods from 7:00 until 20:00. Outside that period comfort bounds are matched with the lower and upper building protect limits which are, respectively, 15°C and 28°C. For convenience, the case study and the considered simulation scenario parameters are summarized in Table I.

Determination of achievable benefits with the proposed BEMS is performed for two typical workday conditions in July covering sunny and semi-cloudy external weather conditions (Scenario A and Scenario B). Heat disturbances in all zones are assumed zero-valued. The expected day-ahead electricity

[1]It stems from internal gains, changed configuration of the zones compared to the state during identification and model inaccuracies.

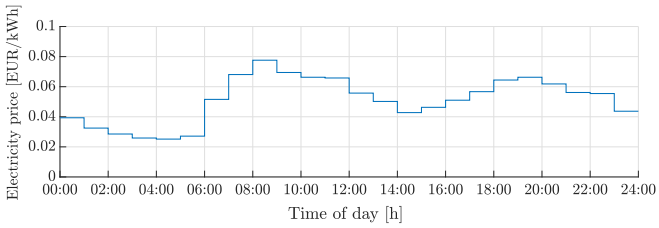

Fig. 3. Day-ahead electricity price profile for grid-building energy exchange.

pricing is shown in Fig. 3, with the price profile obtained from the publicly available European Power Exchange company portal for 2019 [19] and the prices scaled to match the grid fees and supplied energy cost in Croatia [20]. The monthly cost of maximum building power consumption [20] is divided by 30 to represent a correct price amount for single day optimization such that $c_{y^{\mu}_{\max}} = 0.116$ € /kW. Battery system degradation costs of 0.226 € /kWh both for charging and discharging are calculated from the manufacturer's datasheets [32]. In both scenarios, the following control strategies are considered:

1) Baseline Control: The zone-level baseline control is based on a simple hysteresis control of zone temperature with sampling time of 1 min, chosen based on the on-site available commercial equipment. The baseline controller switches between available power outputs based on the difference between the temperature reference and the zone temperature, such that zone's fan coil speed 1 is switched on at −0.15 °C, speed 2 at −0.30 °C and speed 3 at −0.45 °C. The maximum attainable thermal power at the highest fan speed is matched with zone level thermal power limitations used in (3). For a fair comfort level comparison, the baseline controller starts to operate 1 h before the start of the occupancy period to meet the comfort requirements in occupancy periods on time. On the central HVAC system level baseline control constantly keeps the supply temperature at 7.5 °C according to the established practice of the chiller maintenance service. The baseline for the microgrid level control is a simple transactive controller: if the consumed energy is higher than the expected daily average energy consumption, the battery will be discharged with the maximum allowed power; if the consumed energy is lower than the expected daily average consumption, the battery will be charged with the maximum allowed power.

1) Energy-Optimal (EO) Control: In energy-optimal control the BEMS operates in an uncoordinated manner where each building optimization level operates independently (local-wise optimal) with only needed information provided to the upper level. Consequently, the zone level and central HVAC system level optimize their behavior with respect to the energy consumption only ($c_{\mathrm{t}} = \mathbf{1}$, $c_{\mathrm{e}} = \mathbf{1}$). In such a set-up the zone level consumption is a non-controllable load for the central HVAC system level. Likewise, the consumption of the overall HVAC system adds up in a non-controllable way to the non-controllable load and PV production of the microgrid.

1) Price-Optimal (PO) Control: BEMS levels are coordinated according to Algorithm 1.

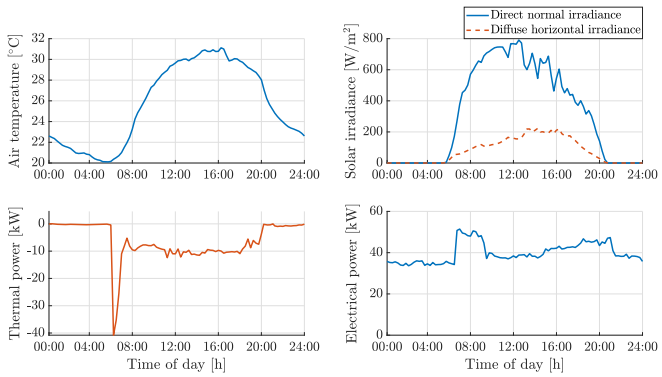

Fig. 4. Considered temperature, solar irradiance, HVAC non-controllable consumption and microgrid net non-controllable consumption that also includes PV system production in scenario A.

The performance of all considered control strategies is verified in a scenario with the enforced repeated behaviour from day to day, i.e., the initial state of the building (at the beginning of the day, at midnight), which is subject to optimization, is equal to the final state of the building (at the next midnight). Thus, all control problems mentioned have for this daily scheduling scenario also the initial state x_0 as the optimization variable. In this way the system does not exploit any initial condition in the building for inducing savings, but leaves the building in the same condition as it was at the beginning of the day – i.e. no energy accumulated in initial conditions is exploited. The repeatability of the baseline controller operation is ensured by simulating the zone performance over several days with the same weather conditions as in the considered simulation scenario. The repeatability of building behaviour in MPC approaches is ensured by adding the following equality constraints to the zone level and the microgrid level optimization problems (4) and (14):

$$x_N^{\mathrm{z}} = x_0^{\mathrm{z}}, \quad x_N^{\mu} = x_0^{\mu}, \tag{27}$$

where $x_0^{\mathrm{z}} \in \mathbb{R}^{n_x^{\mathrm{z}}}$ and $x_0^{\mu} \in \mathbb{R}^{n_x^{\mu}}$ are the initial system states at 0:00 and $x_N^{\mathrm{z}} \in \mathbb{R}^{n_x^{\mathrm{z}}}$ and $x_N^{\mu} \in \mathbb{R}^{n_x^{\mu}}$ are the predicted system states at the end of the prediction horizon of length N, at 24:00. All the MPC controllers operate with 15-min sampling time ($T_{\mathrm{s}} = 15$ min) and thus $N = 96$ for all levels.

In all computations an i7 CPU (i7-5960X) computer with 32 GB RAM was used. The algorithms are implemented in Python with IBM CPLEX [33] used as the LP solver.

D. Simulation Scenario a

Simulation scenario A concerns a sunny day and is determined by external weather and non-controllable consumption on the central HVAC system and microgrid level, see Fig. 4.

First, the potential building operation cost savings with high comfort demands are examined, with comfort-savings trade-off parameter $\gamma = 1$. The possible savings are then discussed in detail at the end of the subsection by considering the relaxation of the users comfort through changing the parameter γ.

1) The Zones Level: Temperature profiles from two exemplary zones, obtained by applying different control strategies for zone temperature control are shown in Fig. 5 and Fig. 6.

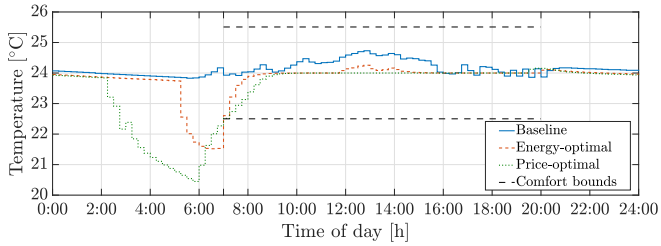

Fig. 5. Air temperature responses in a first exemplary zone selected from the 248 case-study building zones within the analysed day.

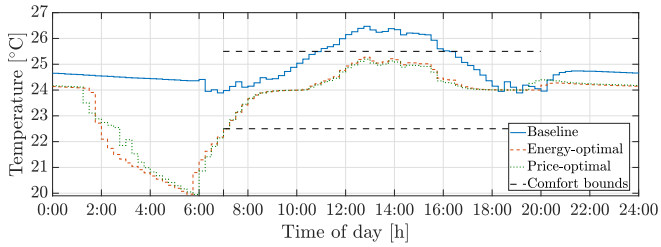

Fig. 6. Air temperature responses in a second exemplary zone selected from the 248 case-study building zones within the analysed day.

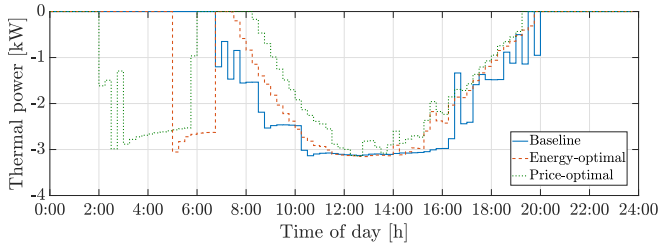

Fig. 7. Cooling needs in the first exemplary zone selected from the 248 building zones within the analysed day.

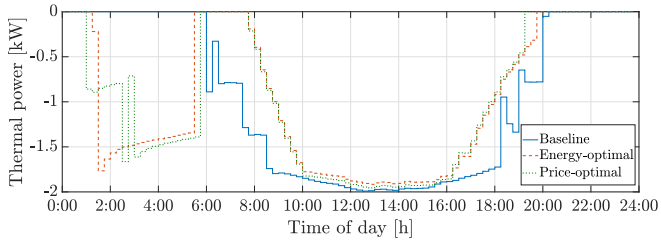

Fig. 8. Cooling needs in the second exemplary zone selected from the 248 case-study building zones within the analysed day.

The responses of the cooling powers exerted into the selected building zones through FCUs averaged on 15-minutes time intervals are shown in Fig. 7 and Fig. 8. The control actions of the baseline controller are based only on current measurements resulting with reactive control and significant disruption of the comfort in zones in which the comfort constraints cannot be satisfied without the appropriately applied pre-cooling actions.

A comparison among the analyzed control strategies of 15-minutes mean thermal power generated from FCUs to zones air in all 248 zones is shown in Fig. 9. Pre-cooling actions enable that the comfort is ensured during the entire day even

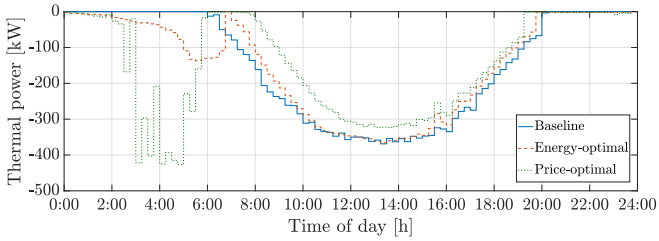

Fig. 9. Overall cooling energy needs for all the zones.

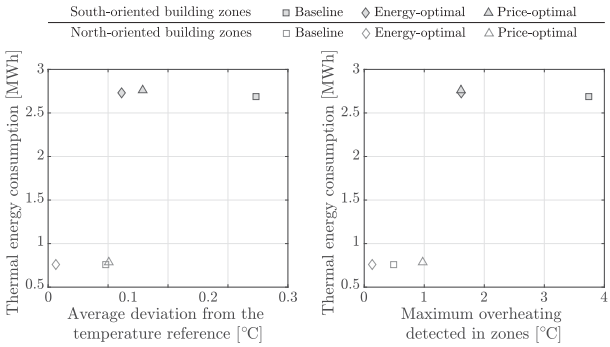

Fig. 10. Comfort level indicators for different controller configurations.

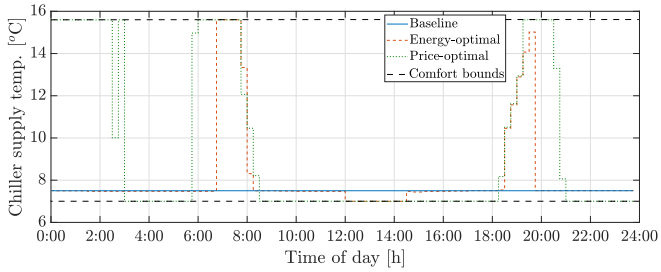

Fig. 11. Comparison of day-ahead supply medium temperature references.

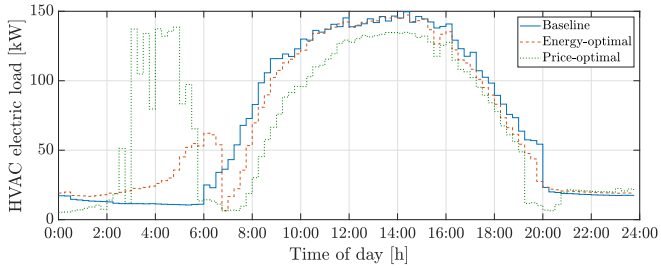

Fig. 12. Comparison of HVAC electrical load profiles.

with the limited power of the cooling system. In case of price-optimal control the microgrid and the central HVAC system level force the zones to additionally shift the thermal energy demand from intervals with higher electricity prices and peaking power demand towards the intervals with more beneficial electrical energy prices and HVAC system efficiency.

In the considered case of seasonal cooling, the comfort with baseline control is significantly disrupted in cases when the available thermal power of fan coils is insufficient to cover the peak demand. Comfort levels parted to north- and south-facing zones are shown in Fig. 10 and compared with the resulting energy consumption of the considered zones. The comfort level indicator, measured as average deviation (AD) from the temperature reference is calculated as:

$$\mathrm{AD} = \frac{1}{n_s n_y^{\mathrm{z}}} \sum_{k \in \mathcal{O}} \| y_{\mathrm{ref},k}^{\mathrm{z}} - y_k^{\mathrm{z}} \|_1, \tag{28}$$

where $\mathcal{O}$ is the set of all the time samples within the occupancy periods and n_s is its cardinal number.

The comfort level indicator provides information on average expected temperature in each time instant, e.g. for price-optimal control with $\Delta_{\mathrm{ref}}^{\mathrm{z}} = 1.5\,^{\circ}\mathrm{C}$, the expected temperature in south-oriented zones for the considered simulation scenario is within the $\pm 0.15\,^{\circ}\mathrm{C}$ range around $y_{\mathrm{ref}}^{\mathrm{z}}$. Additionally, performance of different control strategies is also in Fig. 10 compared with respect to the maximum overheating, i.e. maximum temperature above the reference detected in the building during the occupancy periods. The large overheating of south-oriented zones when using the baseline control strategy is a clear result of lacking predictive feature. In both MPC-based approaches, the temperature in all the building zones is kept within the permissible temperature range of $y_{\mathrm{ref}}^{\mathrm{z}} \pm \Delta_{\mathrm{ref}}^{\mathrm{z}}$, reducing thus the overheating up to 56% and improving the overall comfort in the building zones by at least 57% when compared with the baseline control strategy.

2) The Central HVAC System Level: The day-ahead formation of the supply medium temperature reference at the central HVAC system level is depicted in Fig. 11. The upper and the lower reference limits are denoted with dashed black lines.

An emphasized difference in operation is evident between the central HVAC system energy- and price-optimal controllers in figs. 11 and 12. The decrease of the thermal loads in the zones results in an increase of the supply medium temperature reference, and in combination they bring higher EER of the chiller operation and lower supply pipes thermal losses. During the time instants with the increased thermal loads in the zones, i.e. in the pre-cooling period and in the middle of the day, is the supply medium temperature reference kept close to the minimum allowed reference value.

The electrical load profile of the HVAC system is shown in Fig. 12. The consumption with the employed baseline controller is the lowest in the morning and evening hours, whereas it also has the highest peak The price-optimal control minimizes the peak power value at time instants with the highest loads at the expense of the increased pre-cooling operation in the morning hours when the considered volatile electrical energy prices are the lowest (Fig. 3) and chiller the most efficient. With the abrupt increase of the electrical energy price at 6:00, the central HVAC system controller suddenly reduces the power consumption, which also can be observed in the increase of the supply medium temperature reference in Fig. 11. In respective time instants, the thermal energy request from the zones is reduced, also as a consequence of the employed coordination (see Fig. 9).

3) Microgrid Level: Daily energy exchange with the distribution grid is depicted in Fig. 13. The overall day-ahead

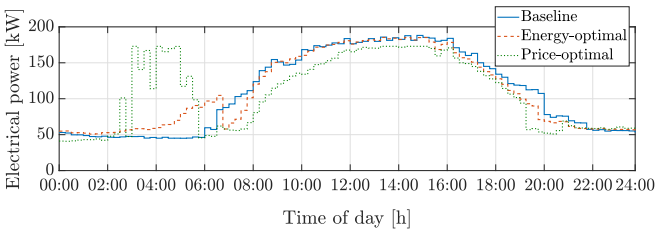

Fig. 13. Overall building power consumption from the electricity grid.

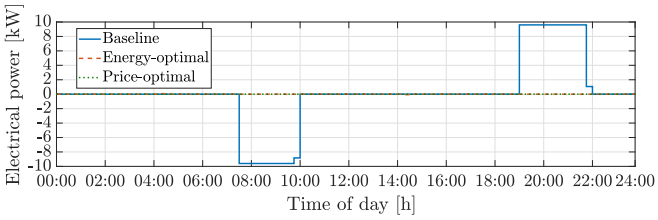

Fig. 14. Battery storage charge and discharge energies profile.

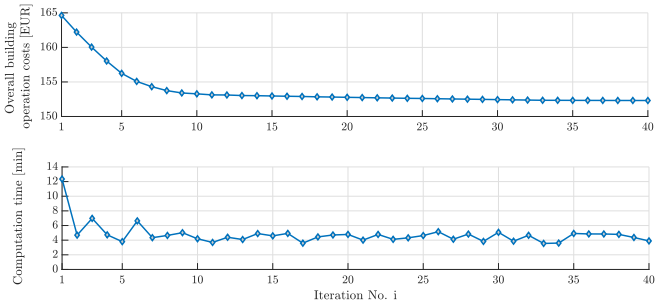

Fig. 15. Daily building operation costs in the upper subplot and the computation times through iterations of the Algorithm 1 in the lower subplot (PO, $\gamma = 1$).

building consumption is adjusted to utilize the price volatility for decreasing the overall operation costs.

Battery storage system charge and discharge energies throughout the day are depicted in Fig. 14 for the three considered control strategies. In the MPC strategies, the batteries are not utilized for additional energy savings due to the combination of their efficiency and the included degradation costs.

4) The Overall Building Operation: Microgrid level cost reduction through iterations of the parametric coordination algorithm is depicted in the upper part of Fig. 15. The overall building operation costs amount to: 179.08 € for the conventional baseline strategy, 164.63 € for the energy-optimal building operation and 152.29 € for the hierarchically coordinated, price-optimal building operation, giving costs reductions of 15%.

The computation times through the iterations of the proposed algorithm are shown in the lower graph of Fig. 15. The algorithm has a blind start (see Algorithm 1) and in iteration $i = 0$ also the energy-optimal solutions for zone and central HVAC levels are computed. In cases of highly volatile energy prices, low battery utilization cost and/or large peak power, these energy-optimal solutions substantially differ from the final results of the optimization which resemble the price-optimal behavior. As a result the number of iterations required for algorithm to converge

TABLE II
THE OVERALL BUILDING OPERATION COSTS (SIMULATION SCENARIO A)

		Operation costs [€]	AD all zones [°C]	AD south [°C]	AD north [°C]	Max. overheating [°C]
Baseline	w Batt	179.08	0.25	0.35	0.10	3.74
	w/o Batt	167.75	0.25	0.35	0.10	3.74
$\gamma = 1$	EO	164.63	0.08	0.12	0.01	1.62
	PO	152.29	0.14	0.16	0.10	1.50
$\gamma = 0.5$	EO	164.89	0.09	0.13	0.01	1.62
	PO	147.17	0.28	0.30	0.25	1.61
$\gamma = 0$	EO	161.75	1.40	1.36	1.47	1.62
	PO	138.91	1.11	1.18	0.99	1.61

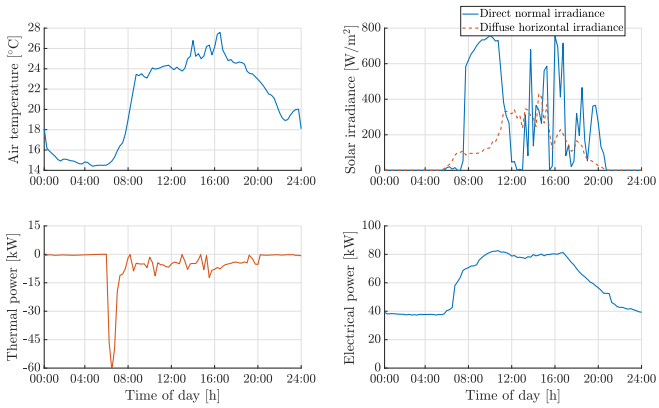

Fig. 16. Considered temperature, solar irradiance, and HVAC non-controllable consumption and microgrid net non-controllable consumption that also includes PV system production for scenario B.

is higher than the number of iterations required for algorithm to converge when applied in a standard receding horizon closed-loop fashion in which the coordination could start from the price-optimal solution calculated at the previous time instant. In [15] it was shown that receding horizon implementation of hierarchical MPC during the whole year never needed more than 3 iterations to converge, in vast majority of cases 1 iteration was enough. Thus, 3 iterations before convergence that cumulatively last less than 15 minutes, imply the feasibility of receding horizon control implementation.

Table II shows the different possibilities of comfort-savings weighing of MPC through parameter γ and two different baseline cases with and without batteries. The considered MPC approaches show better results than the baseline controller due to the prediction of the comfort requirements and timely applied pre-cooling. Even for the case with completely omitted reference following part, with $\gamma = 0$, both considered MPC approaches significantly reduce the maximum overheating occurring with the baseline controller.

E. Simulation Scenario B

Simulation scenario B concerns a semi-cloudy day and is determined by external weather and non-controllable consumption on the central HVAC system and microgrid level, see Fig. 16.

TABLE III
THE OVERALL BUILDING OPERATION COST (SIMULATION SCENARIO B)

		Operation costs [€]	AD all zones [°C]	AD south [°C]	AD north [°C]	Max. overheating [°C]
Baseline	w Batt	182.86	0.20	0.18	0.24	1.53
	w/o Batt	171.50	0.20	0.18	0.24	1.53
$\gamma = 1$	EO	166.97	0.12	0.07	0.20	1.50
	PO	155.94	0.24	0.19	0.32	1.50
$\gamma = 0.5$	EO	166.93	0.12	0.07	0.21	1.50
	PO	145.84	0.53	0.53	0.52	1.50
$\gamma = 0$	EO	160.76	1.36	1.43	1.24	1.50
	PO	138.27	1.10	1.22	0.88	1.50

The different possibilities of comfort-savings weighing through parameter γ on the selected semi-cloudy day are shown in Table III.

The presented results show promising savings possibilities, reaching up to 24% cost reduction for the specified case study scenarios. Each level of the presented modular control system contributes to savings increase, while keeping the possible implementations of the control system flexible and adaptable to various building configurations. Additionally, the achieved thermal comfort in building zones is kept within the defined limits and is substantially improved over the conventional baseline scenario. For the considered predictive control application scenarios, the software-based coordination with utilization of building thermal energy storage achieves the cost-optimal energy management without utilization of the available battery storage system.

V. CONCLUSION

The paper introduces a methodology for multi-level hierarchical model predictive control. Coordination between the hierarchy levels is achieved by utilizing computationally low-cost procedures from multi-parametric programming. Application in building energy management systems (BEMSs) is shown. Coordination of the control levels of comfort in zones, heating/cooling medium preparation and building microgrid is achieved for attaining minimum building operation costs with maintained comfort. Hierarchical structuring enables to keep the control problems of individual levels separated for easier commissioning and maintenance as well as for easy temporary bridging of certain levels where smart controls are not applied. Operation of the proposed BEMS is compared versus the operation of BEMS with non-coordinated model predictive controls on different levels and versus the operation of BEMS with rule-based controls. Real building case study (248 zones, 10.000 m^2) for daily operation scheduling is considered. Significant operation costs reductions are achieved that can be directly attributed to the established coordination mechanism. The introduced hierarchical control can be further extended for provision of demand response services towards energy grid entities as well as for cooperation between buildings within energy communities.

REFERENCES

[1] "Renewable energy policy network for the 21st century (REN21)," Renewables 2019 Global Status Report, 2019.

[2] M. Gruber, A. Trüschel, and J.-O. Dalenbäck, "Model-based controllers for indoor climate control in office buildings - complexity and performance evaluation," *Energy Buildings*, vol. 68, pp. 213–222, 2014.

[3] M. Razmara, M. Maasoumy, M. Shahbakhti, and R. Robinett, "Optimal exergy control of building HVAC system," *Appl. Energy*, vol. 156, pp. 555–565, 2015.

[4] A. Afram and F. Janabi-Sharifi, "Theory and applications of HVAC control systems - A review of model predictive control (MPC)," *Building Environ.*, vol. 72, pp. 343–355, 2014.

[5] D. Sturzenegger, D. Gyalistras, M. Morari, and R. S. Smith, "Model predictive climate control of a swiss office building: Implementation, results, and cost-benefit analysis," *IEEE Trans. Control Syst. Technol.*, vol. 24, no. 1, pp. 1–12, Jan. 2016.

[6] T. Hilliard, L. Swan, and Z. Qin, "Experimental implementation of whole building MPC with zone based thermal comfort adjustments," *Building Environ.*, vol. 125, pp. 326–338, 2017.

[7] S. Yang *et al.*, "Experimental study of a model predictive control system for active chilled beam (ACB) air-conditioning system," *Energy Buildings*, vol. 203, 2019, Art. no. 109451.

[8] F. Bünning, B. Huber, P. Heer, A. Aboudonia, and J. Lygeros, "Experimental demonstration of data predictive control for energy optimization and thermal comfort in buildings," *Energy Buildings*, vol. 211, 2020, Art. no. 109792.

[9] F. Tahersima, J. Stoustrup, H. Rasmussen, and S. A. Meybodi, "Economic COP optimization of a heat pump with hierarchical model predictive control," in *Proc. 51st IEEE Conf. Decis. Control*, 2012, pp. 7583–7588.

[10] D. Setlhaolo, S. Sichilalu, and J. Zhang, "Residential load management in an energy hub with heat pump water heater," *Appl. Energy*, vol. 208, pp. 551–560, 2017.

[11] K. Klein, S. Herkel, H.-M. Henning, and C. Felsmann, "Load shifting using the heating and cooling system of an office building: Quantitative potential evaluation for different flexibility and storage options," *Appl. Energy*, vol. 203, pp. 917–937, 2017.

[12] A. Roskilly, P. Taylor, and J. Yan, "Energy storage systems for a low carbon future - in need of an integrated approach," *Appl. Energy*, vol. 137, pp. 463–466, 2015.

[13] A. Parisio, E. Rikos, and L. Glielmo, "A model predictive control approach to microgrid operation optimization," *IEEE Trans. Control Syst. Technol.*, vol. 22, no. 5, pp. 1813–1827, Sep. 2014.

[14] M. Ruiz-Cortes *et al.*, "Optimal charge/discharge scheduling of batteries in microgrids of prosumers," *IEEE Trans. Energy Convers.*, vol. 34, no. 1, pp. 468–477, Mar. 2019.

[15] V. Lešić, A. Martinčević, and M. Vašak, "Modular energy cost optimization for buildings with integrated microgrid," *Appl. Energy*, vol. 197, pp. 14–28, 2017.

[16] N. Hure, A. Martinčević, and M. Vašak, "Model predictive control of building HVAC system employing zone thermal energy requests," in *Proc. 22nd Int. Conf. Process. Control*, 2019, pp. 13–18.

[17] A. Martinčević, F. Rukavina, V. Lešić, and M. Vašak, "Comfort control in buildings with adherence to the required thermal energy input in zones," in *Proc. IEEE Int. Symp. Ind. Electron.*, 2017, pp. 1477–1482.

[18] M. Vašak and G. Kujundžić, "A battery management system for efficient adherence to energy exchange commands under longevity constraints," *IEEE Trans. Ind. Appl.*, vol. 54, no. 4, pp. 3019–3033, Jul./Aug. 2018.

[19] EPEX SPOT, "European power exchange electricity index," Accessed: Feb. 11, 2020. [Online]. Available: http://www.epexspot.com

[20] HEP ODS, "HEP distribution system operator," Accessed: Feb. 17, 2020. [Online]. Available: http://www.hep.hr/ods/

[21] American society of heating refrigerating and air-conditioning engineers, "ASHRAE Handbook: Fundamentals," Atlanta, GA, USA, 2009.

[22] A. Ogunjuyigbe, T. Ayodele, and O. Akinola, "User satisfaction-induced demand side load management in residential buildings with user budget constraint," *Appl. Energy*, vol. 187, pp. 352–366, 2017.

[23] A. Martinčević, M. Vašak, and V. Lešić, "Model predictive control for energy-saving and comfortable temperature control in buildings," in *Proc. 24th Mediterranean Conf. Control Automat.*, 2016, pp. 298–303.

[24] J. Cigler, S. Prívara, Z. Váňa, E. Žáčeková, and L. Ferkl, "Optimization of predicted mean vote index within model predictive control framework: Computationally tractable solution," *Energy Buildings*, vol. 52, pp. 39–49, 2012.

[25] A. Martinčević and M. Vašak, "Constrained Kalman filter for identification of semiphysical building thermal models," *IEEE Trans. Control Syst. Technol.*, vol. 28, no. 6, pp. 2697–2704, Nov. 2020.
[26] A. Martinčević, M. Vašak, and V. Lešić, "Identification of a control-oriented energy model for a system of fan coil units," *Control Eng. Pract.*, vol. 91, 2019, Art. no. 104100.
[27] M. Gulin, M. Vašak, and M. Baotić, "Analysis of microgrid power flow optimization with consideration of residual storages state," in *Proc. Eur. Control Conf.*, 2015, pp. 3126–3131.
[28] F. Rukavina and M. Vašak, "Optimal parameterization of a PV and a battery system add-on for a consumer," in *Proc. 11th Int. Symp. Power Electron. Distrib. Gener. Syst.*, 2020, pp. 1–6.
[29] F. Borrelli, A. Bemporad, and M. Morari, "Geometric algorithm for multiparametric linear programming," *J. Optim. Theory Appl.*, vol. 118, no. 3, pp. 515–540, 2003.
[30] "Protected cultural heritage no. Z-5675," *Official Gazzette of the Republic of Croatia No. 120/12, Document 2611*, Oct. 2012.
[31] M. Vašak, A. Starčić, V. Lešić, and A. Martinčević, "Upgrade of a typical office building automation system for enabling open energy management services," in *Proc. Int. Conf. Smart Syst. Technol.*, 2017, pp. 309–314.
[32] GWL Power, "Group CA100AHA Lithium cell batteries," Accessed: Jan. 21, 2020. [Online]. Available: https://www.gwl.eu/
[33] Corp IBM, "IBM ILOG CPLEX 20.1.0 high-performance software for mathematical programming and optimization," 2020. [Online]. Available: https://www.ibm.com/analytics/cplex-optimizer

Mario Vašak (Member, IEEE) received the Ph.D. degree from the University of Zagreb Faculty of Electrical Engineering and Computing (UNIZG-FER), Zagreb, Croatia, in 2007. He is currently a Full Professor with the Department of Control and Computer Engineering of UNIZG-FER and he is leading UNIZG-FER's Laboratory for Renewable Energy Systems. He authored more than 20 articles in international scientific journals and overall more than 100 internationally reviewed articles. His research interest focuses on the domain of dynamic systems predictive control with applications to systems from the low-carbon energy sector. He is the main inventor of the U.S. patent for fault-tolerant control of wind turbine generators and has designed the concept of hierarchical and modular energy management in buildings with integrated microgrids for enabling their economically optimal interoperation. He was the President of Control Systems Chapter of the IEEE Croatia Section in period 2014–2017.

Anita Banjac (Member, IEEE) received the Ph.D. degree from the University of Zagreb Faculty of Electrical Engineering and Computing (UNIZG-FER), Zagreb, Croatia, in 2020. She is currently an Assistant Professor with the Department of Control and Computer Engineering of UNIZG-FER. She has authored or coauthored several scientific and professional papers in the field of building climate control, energy management, model predictive control, identification and hierarchical coordination of building subsystems. Her research interests include the domain of advanced control and estimation algorithms with applications to building systems.

Nikola Hure (Member, IEEE) received the Ph.D. degree from the University of Zagreb Faculty of Electrical Engineering and Computing (UNIZG-FER), Zagreb, Croatia in 2017. He is currently a Senior Researcher with the Department of Control and Computer Engineering of UNIZG-FER. He was a Visiting Researcher with the University of Seville in 2014. His research interests include optimal control, coordinated control and operating envelope protection with application to wind turbine systems, building energy management and other cyber-physical systems.

Hrvoje Novak (Member, IEEE) received the Ph.D. degree from the University of Zagreb Faculty of Electrical Engineering and Computing (UNIZG-FER), Zagreb, Croatia, in 2019. He is currently a Senior Researcher with the Department of Control and Computer Engineering of UNIZG-FER. He has authored and coauthored several scientific and professional papers in the field of model predictive control, hierarchical coordination of large energy systems and forecasting with machine learning techniques. His research interests include the domain of advanced control algorithms with application to large energy consumers (buildings, railway transport) and machine learning based prediction algorithms (buildings, water distribution, agriculture).

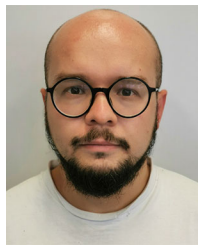

Danko Marušić (Student Member, IEEE) received the M.Sc. degree from the University of Zagreb Faculty of Electrical Engineering and Computing (UNIZG-FER), Zagreb, Croatia, in 2017. He is currently a Ph.D. Student and Researcher with the Department of Control and Computer Engineering of UNIZG-FER. His research interests include control algorithms applied to battery systems in buildings and vehicles.

Vinko Lešić (Senior Member, IEEE) received the Ph.D. degree from the University of Zagreb Faculty of Electrical Engineering and Computing (UNIZG-FER), Zagreb, Croatia, in 2014. He is currently an Assistant Professor with the Department of Control and Computer Engineering of UNIZG-FER. He coauthored more than 40 journal and conference papers and a patent. His research interests include control theory and its application to renewable energy systems and smart city technologies or more particularly, model predictive control for buildings and transport energy efficiency and microgrid operation. He is an Active Volunteer of IEEE Region 8.